Quantification of Loading and Laser-Assisted Release of RNA from Single Gold Nanoparticles

Christoffer Dam Florentsen, Ann-Katrine Vransø West, Helena Maria D. Danielsen, Szabolcs Semsey, Poul Martin Bendix, and Lene B. Oddershede*

Niels Bohr Institute, University of Copenhagen, Blegdamsvej 17, Copenhagen 2100, Denmark

S *Supporting Information*

ABSTRACT: Novel RNA-based technologies provide an avenue of possibilities to control the regulation of gene expression in cells. To realize the full potential of small interfering RNA (siRNA)-based therapy, efficient delivery vehicles and novel strategies for triggering release from carrier vehicles have to be developed. Gold nanoparticles (AuNPs) with sizes of ∼50−150 nm have the ability to accumulate in tumor tissue and can be transported across the membrane by endocytosis. Therefore, a laser-controlled oligonucleotide release from such particles is of particular interest. Here, we quantify the loading of specifically attached microRNA oligonucleotides (miRNA) onto single gold nanoparticles with diameters of 80, 100, 150, and 200 nm. We show that AuNPs have a curvature-dependent density of miRNA loading: the higher the curvature, the higher the loading density. Moreover, we demonstrate how one sensing strand of an RNA duplex can be dehybridized and hence released from the AuNP by heating the AuNP by irradiation with a near-infrared (NIR) laser. Laser-induced release is also demonstrated inside living cells. Together, these findings show that plasmonic nanoparticles with high curvatures are ideal carriers of oligonucleotides into cells, and their cargo can be released in a controlled manner by a thermoplasmonic mechanism. Importantly, this remotely controlled release strategy can be applied to any cargo attached to a plasmonic nanocarrier, on either the single particle or ensemble level.
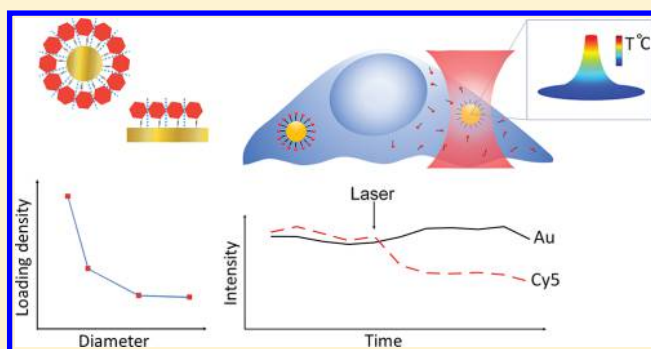
INTRODUCTION

Nanoscale therapeutics holds immense potential for the treatment of diseases with minimal side effects. The development of novel nanoscale drug delivery systems has reached an advanced level with many sophisticated approaches for attaching and releasing a drug, which has been realized in ensemble systems.[1−6] In particular, gold nanoparticles have received significant attention as a nanocarrier system for the following reasons: (i) The gold surface facilitates easy conjugation of ligands, drugs, or oligonucleotides.[7] (ii) Certain sizes of AuNPs will accumulate around tumors if systemically injected and are readily taken up by cells.[8,9] (iii) AuNPs interact strongly with light of specific wavelengths, and the absorption and scattering by AuNPs can be exploited for thermoplasmonic cancer treatment[10] and imaging, respectively. Irradiated AuNPs release their absorbed energy in the form of heat in their local environment.[11] The absorbance of AuNPs is tunable in the optical spectrum, and the shape and composition of AuNPs can be designed to shift the plasmonic band into the NIR region, which coincides with the biological transparency window.[12,13] The prospect of a more efficient cancer treatment using these attractive features of gold nanoparticles for targeted delivery has expanded the field significantly in recent years.[14]

Of special interest for targeted delivery are small RNA oligonucleotides (e.g., siRNA and miRNA), which can be used as a silencer of disease-causing genes.[15] These small RNAs can bind to messenger RNAs (mRNAs) and either prevent or enhance the production of the corresponding translational product.[16,17] Hence, engineered RNA oligonucleotides can be used as a silencer for specific genes in cells. Combining the favorable plasmonic properties of AuNPs with the RNAi pathway by functionalizing the particles with siRNA is a way of creating a drug delivery system which can be activated with light and, at the same time, prevent delivery and the possibly degradation of biomolecules before the target destination has been reached.

Nanostructures such as gold nanoparticles (AuNPs) can be functionalized with several types of biomolecules. These could be deoxyribonucleic acid (DNA), ribonucleic acid (RNA), proteins, or antibodies, which attach by simple and specific chemical conjugation to the gold surface.[7] The loading efficiency has previously been shown in bulk experiments to
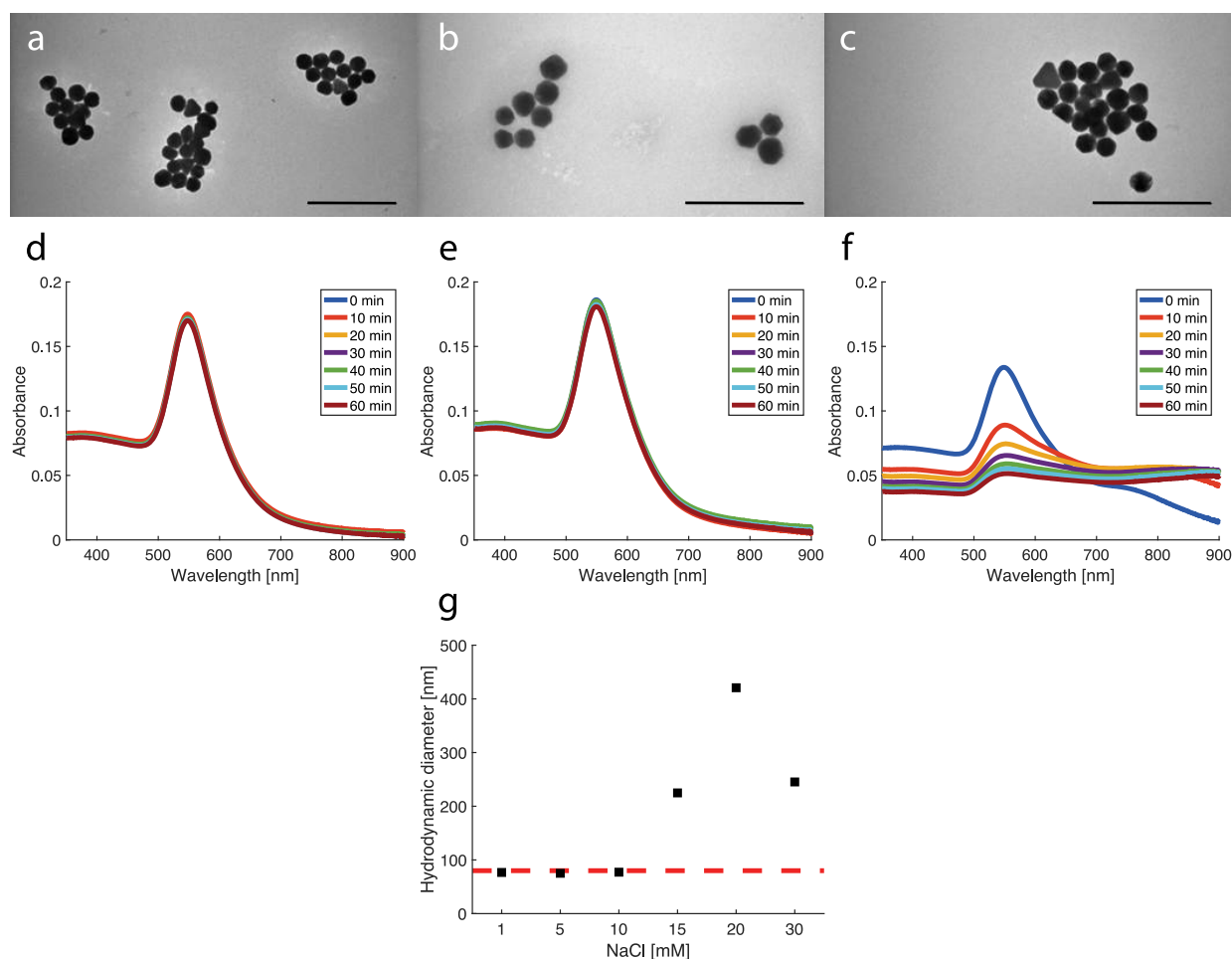
Figure 1. Characterization of bare nanoparticles. (a−c) TEM images of particles used in the study with diameters of (a) 80, (b) 100, and (c) 150 nm. The particles appear to be mostly spherical. Scale bars = 500 nm. (d−f) Absorbance as a function of wavelength for 80 nm AuNPs in TE buffer as a function of time and at varying NaCl concentrations. The NaCl concentrations are (d) 1, (e) 10, and (f) 15 mM. Particles in 1 and 10 mM NaCl appear to be stable with respect to agglomeration; however, particles in 15 mM NaCl show a broadening of the plasmon peak as a function of time, indicating agglomeration. (g) Hydrodynamic diameters of AuNPs (with a nominal diameter of 80 nm) measured by DLS in different NaCl concentrations. The particles appear not to agglomerate at NaCl concentrations of 10 mM or lower. The particles do not seem to agglomerate in low concentrations of salt, but at concentrations above 15 mM NaCl, the average particle size increases, probably due to agglomeration.

depend on the nanoparticle size.[18,19] Furthermore, it has been shown that oligonucleotides can be released from the AuNPs in bulk experiments by irradiation with laser light[20] and from single rotating Au nanorods.[21] However, the bulk experiments do not provide detailed information regarding the single-particle loading efficiency, and the obtained gradual release profile is an average of an ensemble without the quantification of single-particle release profiles. Additionally, the release mechanism may be different in a bulk assay than in single-particle experiments as presented here. The heating from individual AuNPs is negligible at the laser powers used in bulk experiments, but the release can still be caused by a thermal mechanism arising from collective heating from the ensemble. Also, it is possible that heating is caused by photochemical effects.[20] In single-particle experiments, however, because collective effects are not present, the laser power needed to reach a certain temperature will be higher than in ensemble assays. Also, the photochemistry might be different; therefore, laser-induced release on the single-particle level might be quite different from an ensemble assay.

Here, we show how the loading capacity of fluorophore-tagged miRNA with respect to individual gold nanoparticles depends on their surface curvature. Fluorescence from Cy5-miRNA attached to individual AuNPs is quantified for different particle sizes relevant to photothermal cancer treatment; these studies reveal great interparticle variability which cannot be detected in bulk experiments. In addition, we quantify the release of specifically attached miRNA from individual AuNPs in vitro upon irradiation at $\lambda = 1064$ nm, also within living cells. The single-particle assay here presented allows for the quantification of loading efficiency and for the investigation of the mechanism underlying the photothermally induced dehybridization of short nucleotides from nanoparticles. The laser used for triggering release is in the near-infrared biological transparency window, thus making this study relevant by paving the way for in vivo laser-controlled targeted drug release.

■ EXPERIMENTAL SECTION

Materials. All nanoparticles used in this study were purchased from British Biocell International (BBI). The particles were citrate-stabilized and remained nonagglomerated at low ionic solutions.

The AuNP-miRNA construct was made using a thiolated antisense carrier (passenger) strand coupled to the gold surface in conjunction with a nonthiolated functional (guide) sense strand modified with a

fluorescent Cy5 molecule. The fluorescent label allowed for the visualization of the miRNA on the AuNP surface. (sense guide, 5Cy5-GUAGUGCAACAG GGAAAGAGU; passenger antisense, 5Thi-oMC6D-ACUCUUUCCCUGUUGCACUAC). To ensure specific attachment, the thiolated miRNA was reduced using dithiothreitol (DTT). Prior to experiments, the solution was run through a mini quick spin column (Sigma-Aldrich) to separate the DTT from the miRNA

The TE buffer was purchased from Thermo Fischer Scientific, all RNA constructs were purchased from Integrated DNA Technology (IDTDNA), and human embryonic kidney cells (HEK293T) were purchased from ATCC.

Microscopy and Optics. A Leica confocal laser scanning microscope (SP5/TCS) with a 63× water-immersion objective (HC, PL, APO, 63×, NA = 1.20) was used for imaging the nanoparticles and the Cy5-labeled miRNA. The gold nanoparticles were visualized by their scattering of the 514 nm argon laser line. A HeNe laser was applied to excite Cy5 at 633 nm. The Cy5 fluorescence was collected at longer wavelengths (650−770 nm) to minimize crosstalk from both the gold scattering signal and the excitation laser.

The particles were heated using an optical trap (with wavelength λ = 1064 nm) implemented within the confocal microscope. Experimental details of the combined imaging and laser trapping platform are given in ref 22. The irradiating laser intensities were kept in the interval from 20 to 70 mW at the sample. The focused laser was used to irradiate the AuNPs for a few seconds.

Nanoparticle Characterization. Three methods were used to characterize the size of the nanoparticles and possible agglomerates: transmission electron microscopy (TEM), dynamic light scattering (DLS), and UV−vis spectrophotometry. The DLS experiments were carried out using a Malvern Zetasizer Nano DLS, and the measurements were made after the particles had been incubated for 1 h in their respective NaCl suspensions. Figure 1a−c shows TEM images of the particles directly from their stock solutions before adding any electrolytes to the solutions. The particles are spherical, with sizes in accordance with the numbers stated by the manufacturer.

For the stability measurements, the nanoparticles were spun down in an eppendorf tube at 9000 rpm for 5 min. TE buffers with NaCl concentrations of 1, 10, 15, and 30 mM were prepared. The pellet was resuspended in TE buffer with the appropriate NaCl concentration. The absorbance of the samples was monitored every 10 min for 1 h (Figure 1d−f).

In Vitro Release Experiments. For the release experiments, we used miRNA labeled with Cy5 and the following protocol: the AuNP solution was spun down in an eppendorf tube at 9000 rpm for 10 min. The AuNPs were introduced onto a sterile glass surface and left for half an hour to settle on the bottom. NaCl (30 mM) in TE buffer was added 15 min prior to miRNA addition. The miRNA duplex incubated with DTT was run through a mini quick spin column to separate the DTT from the miRNA. This solution and 300 mM NaCl in TE buffer were added to the glass surface containing the AuNPs and left overnight to attach to the AuNPs. The sample was carefully washed using TE buffer before measurements to decrease the background signal. Confocal microscopy was used for imaging the particles, and they were monitored for approximately 10 s after irradiation.

Coverage Experiments. For the coverage experiments we used Cy5-labeled miRNA oligonucleotides and the following protocol: open chambers were made on sterile glass slides with vacuum grease. TE buffer (containing 30 mM NaCl) and gold nanoparticles were added to the chamber and incubated at room temperature for 30 min to allow the particles to settle on the surface. The 30 mM TE buffer was then removed and replaced with another TE buffer containing 300 mM NaCl. The reason for exchanging the salt concentration in the TE buffer is that the particles agglomerate at high salt concentration; however, when they have settled onto the surface in an individual manner a higher salt concentration will facilitate miRNA loading.[18] Hence, after the exchange of TE buffer, an excess of the miRNA duplex was added to the solution and allowed to self-assemble onto the AuNPs for 1 h. Then the samples were carefully washed with 300 mM NaCl TE buffer before imaging to minimize Cy5 background noise. For each particle size, a series of 10 images of different areas were taken for at least 2 different samples done on different days.

miRNA Functionalization. For the functionalization of particles used for release experiments, the particles were spun down in an eppendorf tube at 9000 rpm for 5 min, and then the miRNA duplex was treated with DTT and run through a quick spin column. For the cellular experiments, the particles were mixed with the AuNP solution and the AuNP-miRNA complex was resuspended in TE buffer with 30 mM NaCl and left stirring overnight (1.5 h at 37 °C, thereafter at 4 °C) before using them to flush the chamber with cells.

Intracellular Release Experiments. For the intracellular release experiments, the particles with miRNA were prepared as described under "miRNA functionalization". In order to remove excess miRNA, the supernatant was removed, after which 30 mM NaCl TE buffer was added to a total volume of 80 μL. An Ibidi μ-slide 8-well cell plate was prepared the day before imaging with ~15 000 HEK293T cells per well in excess medium. Four hours before imaging, ~4 × 10^8 functionalized particles were added to each microwell. Imaging and particle heating were done as described in the in vitro release experiments, and the laser intensity was approximately ~30 mW.

Data Analysis. Confocal images were acquired by the Leica Application Suite software and subsequently exported as tiff files for analysis in Matlab (The MathWorks, Natick MA). Fluorescence intensities from single gold nanoparticles carrying Cy5-labeled miRNA were quantified by custom-made algorithms written in Matlab. To this end, a global threshold was applied to the image to localize fluorescent particles. An area threshold of four pixels was applied to discriminate single-pixel noise from real Cy5 signals. Since images typically have a slight intensity gradient in the background, we subsequently used an automated Matlab function to fit a 2D Gaussian function to each intensity spot. The Gaussian fit allowed us to set a local intensity threshold around each nanoparticle for accurate quantification of the Cy5 intensity. The summation of all pixel intensities within each cluster represented the total Cy5 intensity from each nanoparticle. Importantly, to discriminate agglomerates (dimers, trimers, etc.) from single nanoparticles, we fitted an ellipse to each pixel cluster and applied an ellipticity threshold, Tr, defined as $Tr = \frac{Ma - Mi}{Ma + Mi} < 0.3$, where Ma is the major axis and Mi denotes the minor axis of the ellipse. All software reported in this article is available on request.

■ RESULTS AND DISCUSSION

The overall goal of the current study is to show how a AuNP construct can be used as a remotely controlled transporter of biomolecules, e.g., of functional miRNA or siRNA, both in vitro and inside living human embryonic kidney cells (HEK293T). This study aims at investigating laser-induced release from nanoparticles which are relevant carriers inside living organisms. To be relevant carriers, the particles need to absorb reasonably well in the NIR regime because this is the biological transparency window. Also, the particles need to be nontoxic, thermally stable, and available in high biocompatible quality, and they need to have a high degree of accumulation in tumor tissue by the enhanced permeability and retention effect (EPR).[23,24] Therefore, we have chosen to investigate solid gold nanoparticles with diameters of 80, 100, and 150 nm. These particles have been shown to absorb NIR irradiation in a sufficient manner[11] to reach the dehybridization temperature range of the RNA duplex used here, and in addition, these nanoparticles have been shown to serve well in photothermal cancer therapy.[10] The 150 nm NIR resonant gold nanoshell is also an excellent candidate for photothermal therapy,[10] although it is not fully thermally stable at the intensities used here.[25] Because the gold nanoshell has the same diameter as
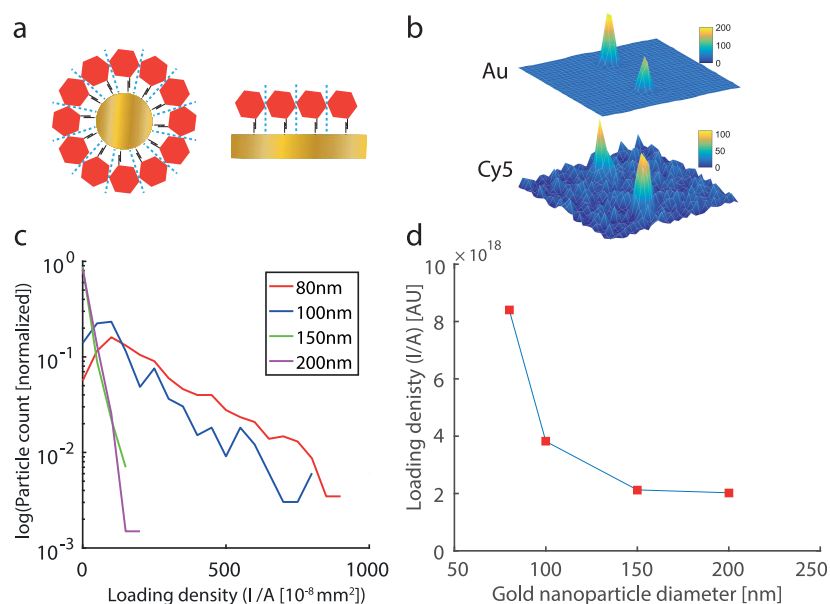
Figure 2. Curvature-dependent loading of Cy5-labeled miRNA on single AuNPs of different sizes. (a) Sketch of the difference between loading bulky molecules on a highly curved surface (left) and a planar surface (right). (b) Surface intensity plots of AuNPs coated with Cy5-miRNA, with the top image showing the scattering confocal image of gold and the lower image showing the Cy5 emission as obtained by confocal microscopy. (c) Number of particles as a function of Cy5 intensity on the particle normalized by the particle's area. (d) Integrated loading intensity as a function of particle size. There is a larger Cy5 loading capacity per area on the smaller particles with higher curvatures. The number of particles used for each type of experiment was $n = 1153$ for 80 nm AuNPs, $n = 330$ for 100 nm AuNPs, $n = 857$ for 150 nm AuNPs, and $n = 669$ for 200 nm AuNPs.

the largest particle in the current study, it is likely that the loading and release mechanisms found here could also be valid for the gold nanoshell. We first investigate under which electrolyte conditions the particles are stable with respect to agglomeration, then we focus on the molecular loading capacity of nanoparticles as a function of particle curvature, and finally we demonstrate a laser-controlled release of the loaded molecules from the nanoparticle both in vitro and inside a living cell.

Stability of Nanoparticles in Electrolyte Solutions. One major obstacle when working with metallic nanoparticles such as AuNPs is their tendency to agglomerate in the presence of salt.[26−28] The Electrostatic screening of surface charges by dissolved ions reduces the Debye length, which sets the range of electrostatic repulsion between particles. Notably, agglomeration is not necessarily unfavorable for cellular uptake as shown in Dykman et al.,[24] but for the reliable quantification of loading a controlled functionalization with single AuNPs, it is important. Hence, the first step toward the functionalization of AuNPs with oligonucleotides and small RNAs is to understand under which conditions the particles agglomerate.

The absorbance of 80 nm bare AuNPs as a function of wavelength at different time points is shown in Figure 1 for NaCl concentrations of (d) 1, (e) 10, and (f) 15 mM. These graphs show that the absorbance does not change as a function of time in 1 or 10 mM NaCl; however, there is a significant broadening of the spectrum as a function of time, possibly due to agglomeration, in the presence of 15 mM NaCl.

To further solidify this result, we performed DLS measurements on the same types of samples. As visible from Figure 1g, the DLS measurements returned a hydrodynamic radius of 80 nm for NaCl concentrations below 10 mM, consistent with the expected results based on the size of bare single particles (80 nm, red horizontal dashed line). However, for NaCl concentrations of 15 mM or higher, the average hydrodynamic

diameter increases, which is a clear sign of particle agglomeration, consistent with the UV−vis measurements shown in Figure 1d−f. These findings show an even lower threshold for agglomeration than what was found by Pamies et al.[26] Therefore, if it is a strict requirement that the AuNPs should be individual and not agglomerated, then the electrolyte concentration should be kept below 10 mM.

Curvature-Dependent Loading of miRNA Duplexes onto AuNPs. Because of the high curvature of the surface of a nanoparticle, it is likely that a nanoparticle can accommodate a larger density of loaded molecules than a planar surface. (See the sketch of these two situations in Figure 2a.) To investigate whether and to what extent miRNA could be loaded onto AuNPs, we monitored the loading of Cy5-labeled miRNA onto AuNPs of varying size. The experimental procedures are described in the Experimental Section. Surface intensity plots from a typical experiment are shown in Figure 2b. The top image shows the gold nanoparticles via reflection confocal microscopy, and the bottom image shows the fluorescent emission from Cy5. The gold signal nicely overlays the Cy5 signal, thus signifying the successful Cy5 labeling of the AuNPs. Quantification of the Cy5 loading on single particles with diameters of 80, 100, 150, and 200 nm is shown in Figure 2c,d. The abscissa on Figure 2c shows the intensity normalized by the particle's projected surface area for the four different particles investigated. Figure 2d shows the integrated loading density as a function of particle diameter, and from Figure 2c,d, it is clear that the smaller the particle (and the higher the curvature), the higher the loading density. The difference in loading capacity is rather steep, going from 80 to 100 nm in diameter, and less steep for the larger particles. Occasionally, small agglomerates may occur. Hence, the analysis uses an ellipticity threshold to identify aggregates and omit these from the analysis.
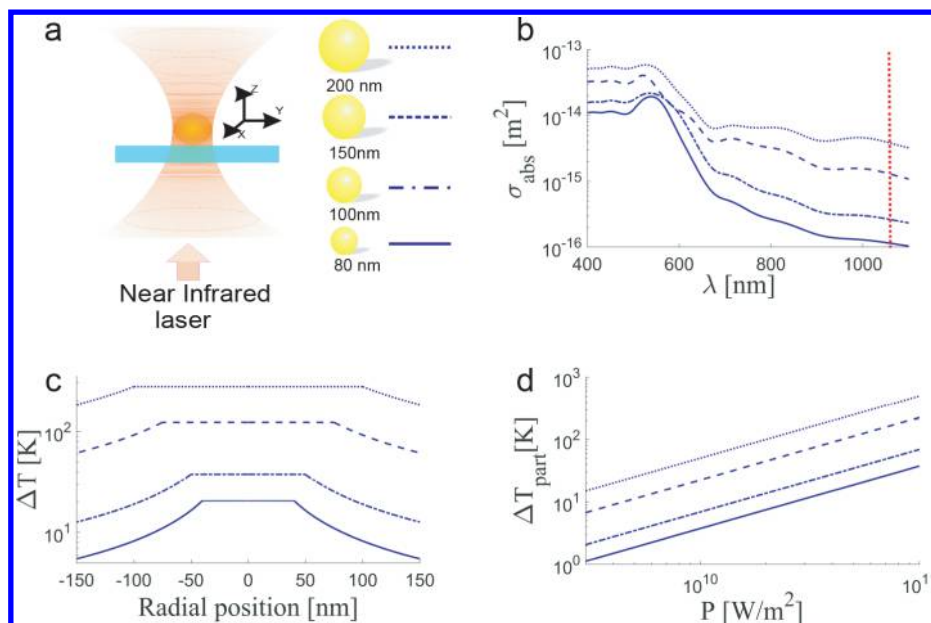
Figure 3. Laser irradiation of individual gold nanoparticles causes the temperature to increase significantly and in a controlled manner. (a) Sketch of focused laser irradiation of a AuNP. (Inset) Schematic of the particles used in the current investigation. (b) Absorption cross sections as a function of wavelength for the particles sketched in panel a. Solid line, 80 nm; dashed−dotted line, 100 nm; dashed line, 150 nm; and dotted line, 200 nm. These line symbols are also used in panels c and d. The vertical dashed red line indicates the irradiating wavelength (1064 nm). (c) Calculated temperature profiles of the particles depicted in panel a irradiated by 150 mW at 1064 nm. (d) Temperature increase at the particle surface versus laser power for the sizes shown in panel a. The simulations of AuNP heating were done using Mie theory as described in ref 11.

The results depicted in Figure 2 are in accordance with ensemble experiments: Hill et al.[18] report that the coverage of nanoparticles with diameters below 60 nm have a strong dependence on curvature, with the smaller particles having a higher coverage density. For particles with diameters above 60 nm, however, the same study showed only a small correlation between curvature and surface coverage, with the coverage being essentially similar to that on a planar surface.[18] Another ensemble study by Hurst et al.[19] demonstrated a positive correlation between nanoparticle curvature and single-stranded DNA surface coverage for nanoparticles with diameters of 15 to 250 nm in accordance with the current single-particle study. Altogether, it does make sense that surfaces with higher curvatures can accommodate a higher density of bulky molecules.

In addition to the observation of increased coverage with smaller particle size for particles of diameters between 80 and 200 nm, we also observe considerable heterogeneity in particle coverage within the same nanoparticle population. This kind of information is uniquely picked up by a single-particle assay and could reflect adsorption kinetics being affected by some underlying causes such as variabilities in the nanoparticle shape and size within the same nominal distribution. One advantage of the single-nanoparticle assay is the ability to detect and even avoid small agglomerations of nanoparticles, which is hard to discriminate in bulk assays. Even small nanoparticle agglomerates can be discriminated by image analysis considering the asymmetry of the intensity distribution from the fluorescent nanoparticles.

In Vitro Release. It has previously been documented that irradiating gold nanoparticles with an NIR laser, as sketched in Figure 3a, leads to very high and localized heating.[11,29] The exact temperature reached depends on the absorption cross sections of the particles, which varies with the particle size and wavelength, as plotted for AuNPs in Figure 3b. The

temperature profile around an irradiated nanoparticle can be accurately calculated by Mie theory or finite element simulations and will generally fall off inversely with distance as depicted in Figure 3c. The information plotted in Figure 3b−d has been calculated using the theory and formulas presented in refs 11 and 30.

Such laser-induced heating of a AuNP can mediate the release of the molecules covering the surface of the AuNP. The surface temperatures of such irradiated AuNPs can easily reach ∼50 to 100 °C above ambient temperature (Figure 3d) and could thereby well be responsible for the dehybridization and release of a Cy5-tagged guide RNA sense strand. The length of the miRNA is 21 base pairs, which gives a melting temperature of ∼53.4 ± 1.3 °C (calculated with the IDTDNA melting temperature applet). This is consistent with a release mechanism in which the double-stranded miRNA covering the AuNP melts and liberates the single Cy5-tagged miRNA strand that is not attached to the AuNP via a thiol bond. It is anticipated that as soon as the melting temperature of the miRNA molecules is reached, the complementary strand is released. The laser powers used for in vitro laser-induced release yield a temperature increase of ∼40 °C above ambient temperature for the 80 nm particles and somewhat higher for the larger particles.[11] Hence, the temperature is high enough at the surface of the irradiated particles to allow for miRNA melting and ss-miRNA release. Irradiation is carried out for only a few seconds to minimize the degradation of the system.

By immobilizing Cy5-miRNA-AuNPs onto a glass substrate and placing them in a setup as sketched in Figure 4a, we monitored the release of Cy5-miRNA molecules from individual AuNPs upon laser irradiation. Images from a typical experiment using 100 nm AuNPs are shown in Figure 4b,c, where panel b shows the signal from gold (upper image) and from Cy5 (lower image) before irradiation and panel c shows the corresponding signals after irradiation. As demonstrated by
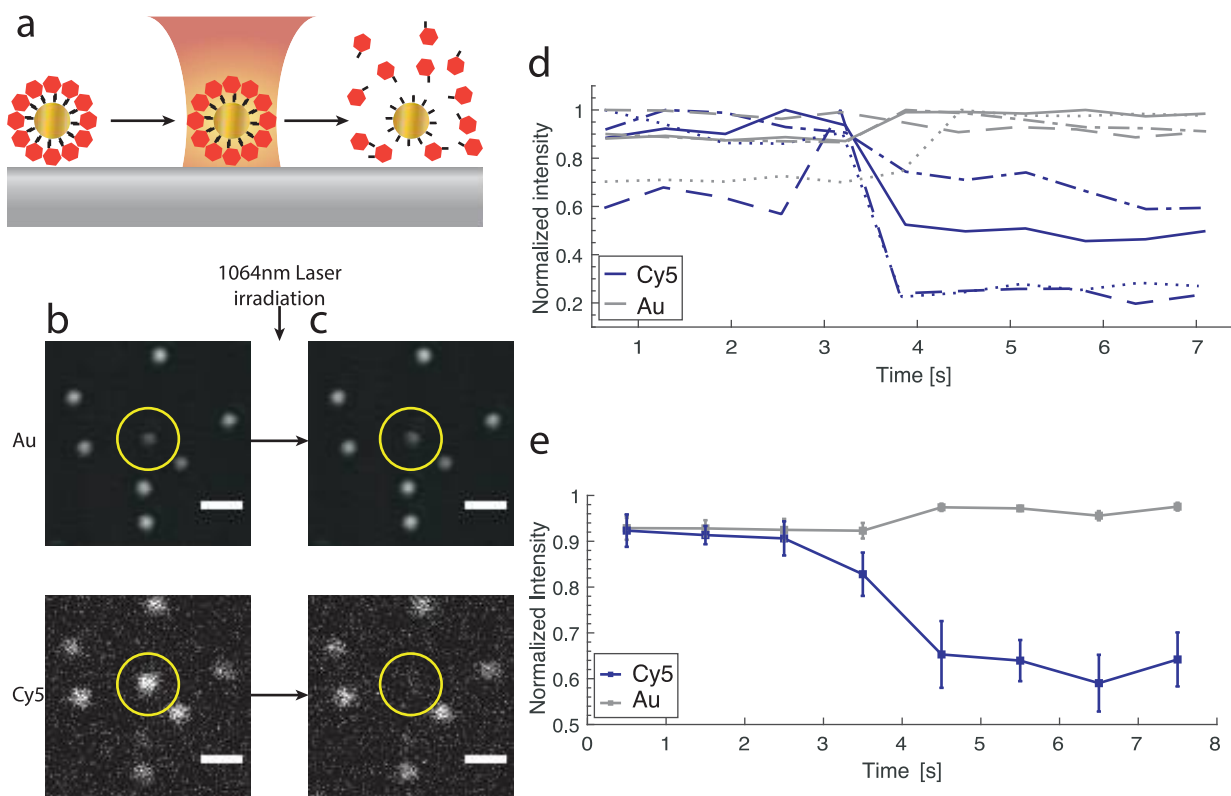
Figure 4. In vitro release of single-stranded Cy5-labeled miRNA from the surface of AuNPs upon laser irradiation. (a) Sketch of the laser-induced release of single-stranded miRNA from AuNPs immobilized on a glass substrate. (b) Confocal images of 100 nm AuNPs (upper image) and the associated Cy5 molecules (lower image) before NIR laser irradiation. The laser irradiated the regions within the yellow circles. (c) Images corresponding to panel b but after NIR laser irradiation, which causes the Cy5 signal to disappear. (d) Quantification of Cy5 and Au signal upon laser irradiation of four representative 100 nm Cy5-miRNA-AuNPs. The gray lines show the bare gold signal, which does not change upon irradiation. The blue lines show the corresponding Cy5 signal from the same four particles upon NIR irradiation. The Cy5 signal decreases significantly and instantaneously upon laser irradiation. The laser intensity used for these experiments was ∼70 mW at the sample. (e) As in panel d but average values from 11 individual experiments. The error bars represent 1 standard deviation of the mean (SEM). All scale bars are 1 μm.

Figure 4b,c, the AuNP does not change visually after irradiation; however, the Cy5 signal does disappear upon irradiation. This is consistent with the laser-induced release of Cy5-miRNA upon laser irradiation. The traces shown in Figure 4d quantify the release of the Cy5 signal from individual AuNPs. The Cy5 signal (blue lines) decreases instantaneously as the NIR laser is turned on. Controls demonstrate essentially no decrease in the Cy5 signal upon confocal excitation and imaging over similar time scales (dotted lines in Supporting Information, Figure S1). Hence, the decreases in Cy5 signals visible in Figure 4d are not due to bleaching of the fluorophore by the imaging laser. Figure 4e shows an average over n = 11 individual traces, the blue line shows the Cy5 signal, which significantly decreases upon laser irradiation, and the gray line shows the gold signal, which stays constant, as expected.

Interestingly, other studies, which have shown successful silencing of GFP expression using gold nanoparticles as carriers of siRNA in ensemble studies, have used laser powers which were up to 6 orders of magnitude lower than used here.[4,20] In the case where nanoparticles are highly abundant, both within and covering cells, collective effects become important and lower laser powers are needed to achieve a certain temperature, compared to the single-particle case, thus partially explaining the observed difference. However, the irradiation time in these ensemble experiments was also much longer (ranging from 10 min[3] to 2 min[4]) than the irradiation times presented here, and this, in combination with the high density of particles, makes

photochemical effects more pronounced. As suggested by the authors,[4,20] photochemistry may be the cause of the low-power release.

Release Inside a Living Cell. To investigate laser-controlled release from nanoparticles inside single cells, we incubated HEK cells with 80 nm Cy5-miRNA-AuNPs, and the release experiments proceeded as sketched in Figure 5a. The cells readily endocytosed the Cy5-miRNA-AuNPs, which were clearly visible inside the cells by reflection confocal microscopy (Figure 5b, top). The Cy5 signal inside the cells was also visible (Figure 5b, bottom) and colocalized with the scattering signal from the gold particles. Hence, it appears that the Cy5-miRNA-AuNP complex was still intact after endocytosis. The endocytosed particles are expected to be located in endosomes, and they are probably somewhat aggregated.[31] Upon NIR irradiation of the Cy5-miRNA-AuNP complex within the cell's cytoplasm, the Cy5 signal decreased while the scattering signal from the AuNPs remained, thus signifying the laser-induced release of Cy5-miRNA from the AuNPs inside the living cell (Figure 5c). In the literature, it has been shown that laser irradiation can cause the melting of the endosomal membrane,[32] and the temperatures reached in the current study will indeed be higher than the phase-transition temperature of biological membranes, hence they are likely to become permeable. After laser irradiation, some fluorescence can still be detected in the area, albeit with a significantly lower intensity than before irradiation. This residual intensity
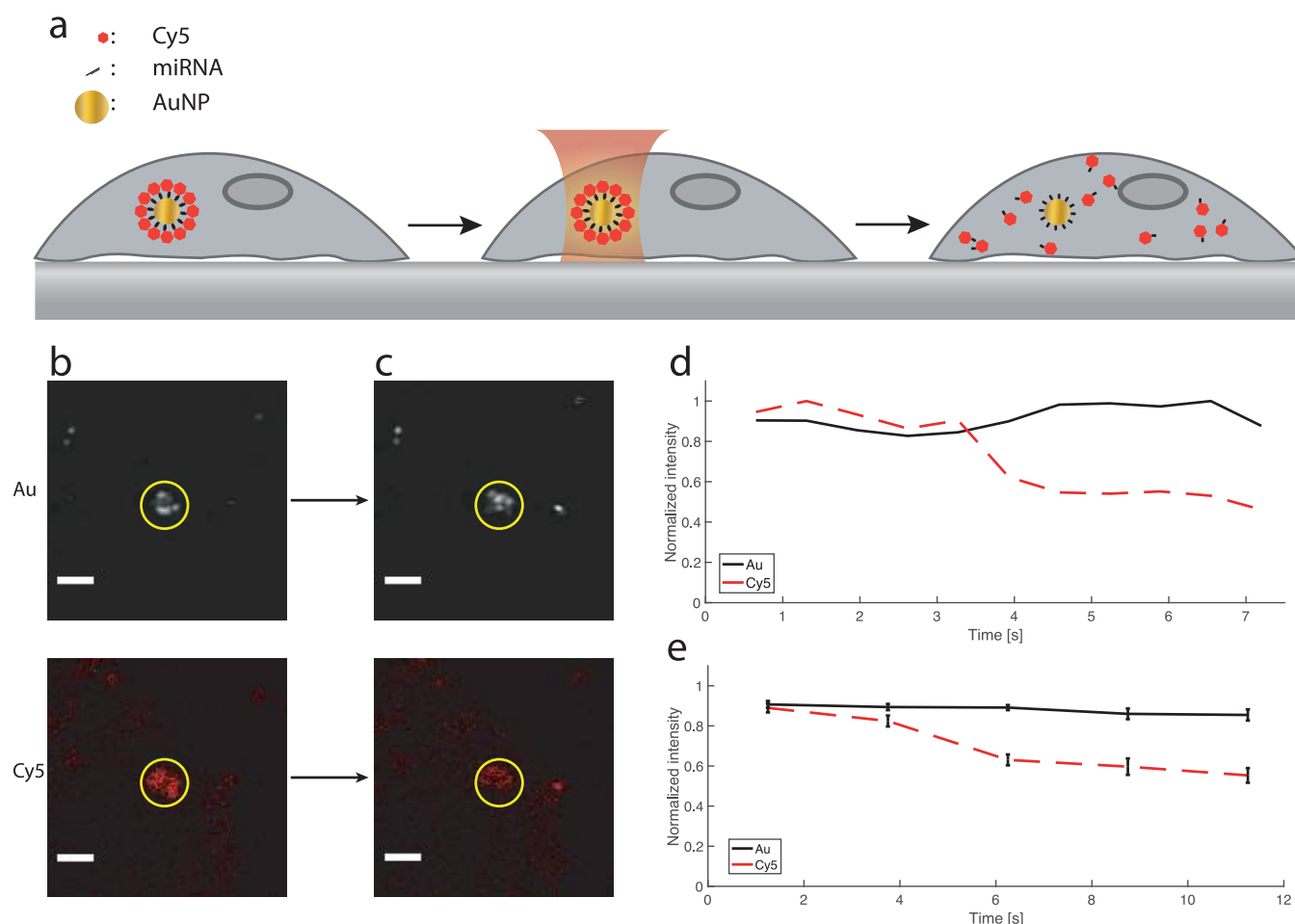
Figure 5. Laser-induced release of single-stranded Cy5-labeled miRNA from AuNPs inside living cells. (a) Sketch of the experiment with a cell immobilized on a glass substrate and the proposed release mechanism. (b) Confocal images of living cells with 80 nm AuNPs (upper image) and associated Cy5 molecules (lower image) before NIR laser irradiation. The scale bar is 2 μm. (c) Images corresponding to panel b but after NIR laser irradiation, which causes the Cy5 signal to decrease. The scale bar is 2 μm. The laser irradiated the regions within the yellow circles, and the laser power was ∼30 mW at the sample. (d) Quantification of Cy5 and gold signal upon laser irradiation of Cy5-miRNA-AuNPs inside a living cell (the same cell as imaged in panels b and c). The black lines show the bare gold signal, which increases slightly upon laser irradiation, possibly due to the trapping effect of the focused laser, which will tend to increase the number of AuNPs in the focus. The red line shows the corresponding Cy5 signal, which decreases upon laser irradiation. (e) The same as in panel d, but average values from 13 individual experiments. Error bars show the standard error of the mean (SEM).

could be due to the fact that the Cy5-miRNA diffuses much less in the crowded cytoplasm than in the test tube, or it could indicate a partial release from the endosome. Also, the cells exhibit autofluorescence in the collected wavelength interval.

Figure 5d shows the scattering signal from gold (black full line) along with the Cy5 signal (red dashed line) during an intracellular release experiment. Figure 5e shows corresponding average curves from 13 individual release experiments. These traces consistently demonstrate a decrease in the intracellular Cy5 signal upon irradiation. There are, however, certain differences in comparison to the in vitro release experiments. For instance, in Figure 5b,d it appears that the gold signal increases slightly upon laser irradiation. This is probably caused by the fact that the gold nanoparticles inside cells often rearrange somewhat upon laser irradiation. This is expected because the particles are not firmly attached to anything and a focused laser operating in this power regime is known to be capable of manipulating and displacing gold nanoparticles of these sizes.[33] For the reasons discussed above and consistent with the lower image in Figure 5c, the Cy5

signal does not go to zero upon laser irradiation but on average decreases only ∼40%.

The cells did not change visually upon laser irradiation. See an example of cell images before and after irradiation in Supporting Information, Figure S2. Hence, the cells did not appear to be physiologically damaged by the release process.

■ CONCLUSIONS

Gold nanoparticles can be used as carriers of double-stranded miRNA constructs. We have shown that the loading capacity of individual gold nanoparticles is dependent on the particle's surface curvature; particles with higher curvatures are able to accommodate a higher density of molecules than particles with lower curvatures. By NIR laser irradiation of the miRNA duplex-AuNP complex, AuNP undergoes substantial heating, thereby melting the double-stranded miRNA and releasing the single strand that is not attached to the AuNP via a thiol bond. Such a release has been demonstrated here on the single-particle level in vitro and inside living cells. Hence, our results demonstrate that it is possible to control miRNA release

remotely with an NIR laser. As NIR lasers have a large penetration depth inside biological tissues and as AuNPs are relatively inert by themselves, these results pave the way for using this mechanism for realizing targeted drug delivery, potentially also inside the human body.

■ ASSOCIATED CONTENT

ⓢ Supporting Information

The Supporting Information is available free of charge on the ACS Publications website at DOI: 10.1021/acs.langmuir.8b01831.

> Control experiment quantifying the degree of Cy5 bleaching in a typical experiment and images of cells before and after laser irradiation (PDF)

■ AUTHOR INFORMATION

Corresponding Author

*E-mail: oddershede@nbi.ku.dk.

ORCID ⓞ

Lene B. Oddershede: 0000-0003-2923-2844

Notes

The authors declare no competing financial interest.

■ ACKNOWLEDGMENTS

■ REFERENCES

(1) Ding, Z. W.; Jiang, Y.; Saha, K.; Kim, C.; Kim, S.; Landis, R.; Rotello, V. M. *Mol. Ther.* **2014**, *22*, 1075−1083.

(2) Jones, M. R.; Seeman, N. C.; Mirkin, C. A. *Science* **2015**, *347*, 1260901−1260901.

(3) Huschka, R.; Neumann, O.; Barhoumi, A.; Halas, N. J. *Nano Lett.* **2010**, *10*, 4117−4122.

(4) Huschka, R.; Barhoumi, A.; Liu, Q.; Roth, J. a.; Ji, L.; Halas, N. J. *ACS Nano* **2012**, *6*, 7681−7691.

(5) Williams, S. *Proc. Natl. Acad. Sci. U. S. A.* **2013**, *110*, 13231−13233.

(6) Goodman, A.; Hogen, N.; Gottheim, S.; Li, C.; Clare, S.; Halas, N. *ACS Nano* **2017**, *11*, 171−179.

(7) Fratila, R. M.; Mitchell, S. G.; del Pino, P.; Grazu, V.; de la Fuente, J. M. *Langmuir* **2014**, *30*, 15057−15071.

(8) Choi, C.; Hao, L.; Narayan, S.; Auyeung, E.; Mirkin, C. *Proc. Natl. Acad. Sci. U. S. A.* **2013**, *110*, 7625−7630.

(9) Giljohann, D.; Seferos, D.; Patel, P.; Millstone, J.; Rosi, N.; Mirkin, C. *Nano Lett.* **2007**, *7*, 3818−3821.

(10) Jørgensen, J. T.; Nørregaard, K.; Tian, P.; Bendix, P. M.; Kjaer, A.; Oddershede, L. B. *Sci. Rep.* **2016**, *6*, 30076.

(11) Bendix, P. M.; Reihani, S. N. S.; Oddershede, L. B. *ACS Nano* **2010**, *4*, 2256−2262.

(12) de Aberasturi, D. J.; Serrano-Montes, A. B.; Liz-Marzán, L. M. *Adv. Opt. Mater.* **2015**, *3*, 602−617.

(13) Weissleder, R. *Nat. Biotechnol.* **2001**, *19*, 316−317.

(14) Ghosh, P.; Han, G.; De, M.; Kim, C. K.; Rotello, V. M. *Adv. Drug Delivery Rev.* **2008**, *60*, 1307−1315.

(15) de Fougerolles, A.; Vornlocher, H.-P.; Maraganore, J.; Lieberman, J. *Nat. Rev. Drug Discovery* **2007**, *6*, 443−453.

(16) Holen, T. T.; Amarzguioui, M.; Babaie, E.; Prydz, H. *Nucleic Acids Res.* **2003**, *31* (9), 2401−2407.

(17) Lam, J. K. W.; Chow, M. Y. T.; Zhang, Y.; Leung, S. W. S. *Mol. Ther.–Nucleic Acids* **2015**, *4*, No. e252.

(18) Hill, H. D.; Millstone, J. E.; Banholzer, M. J.; Mirkin, C. a. *ACS Nano* **2009**, *3*, 418−424.

(19) Hurst, S. J.; Lytton-Jean, A. K. R.; Mirkin, C. a. *Anal. Chem.* **2006**, *78*, 8313−8318.

(20) Huschka, R.; Zuloaga, J.; Knight, M. W.; Brown, L. V.; Nordlander, P.; Halas, N. J. *J. Am. Chem. Soc.* **2011**, *133*, 12247−12255.

(21) Šipova, H.; Shao, L.; Odebo Lank, N.; Andren, D.; Kall, M. *ACS Photonics* **2018**, *5*, 2168−2175.

(22) Richardson, A. C.; Reihani, N.; Oddershede, L. B. *Proc. SPIE* **2006**, *6326*, 632628−632628−10.

(23) Chithrani, B. D.; Ghazani, A. a.; Chan, W. C. W. *Nano Lett.* **2006**, *6*, 662−668.

(24) Dykman, L.; Khlebtsov, N. G. *Chem. Rev.* **2014**, *114*, 1258−1288.

(25) Samadi, A.; Klingberg, H.; Jauffred, L.; Kjaer, A.; Bendix, P.; Oddershede, L. *Nanoscale* **2018**, *10*, 9097.

(26) Pamies, R.; Cifre, J. G. H.; Espín, V. F.; Collado-González, M.; Baños, F. G. D.; de la Torre, J. G. *J. Nanopart. Res.* **2014**, *16*, 2376.

(27) Zhang, X.; Servos, M. R.; Liu, J. *J. Am. Chem. Soc.* **2012**, *134*, 7266−7269.

(28) Albanese, A.; Chan, W. C. W. *ACS Nano* **2011**, *5*, 5478−5489.

(29) Kyrsting, A.; Bendix, P. M.; Stamou, D. G.; Oddershede, L. B. *Nano Lett.* **2011**, *11*, 888−892.

(30) Ma, H.; Tian, P.; Pello, J.; Bendix, P. M.; Oddershede, L. B. *Nano Lett.* **2014**, *14*, 612−619.

(31) Kaluzova, M.; Bouras, A.; Machaidze, R.; Hadjipanayis, C. *Oncotarget* **2015**, *6*, 8788−8806.

(32) Carregal-Romero, S.; Ochs, M.; Rivera-Gil, P.; Ganas, C.; Pavlov, A.; Sukho- rukov, G.; Parak, W. *J. Controlled Release* **2012**, *159*, 120−127.

(33) Hansen, P. M.; Bhatia, V. K.; Harrit, N.; Oddershede, L. *Nano Lett.* **2005**, *5*, 1937−1942.